Detection of tension force reduction in a post-tensioning tendon using pulsed-eddy-current measurement

Ji-Min Kim[a], Jun Lee[a] and Hoon Sohn[*]

Department of Civil Engineering, Korean Advanced Institute for Science and Technology,
291 Daehak-ro, Yuseong-gu, Daejeon 34141, Republic of Korea

Abstract. Post-tensioning (PT) tendons are commonly used for the assembly of modularized concrete members, and tension is applied to the tendons during construction to facilitate the integrated behavior of the members. However, the tension in a PT tendon decreases over time due to steel corrosion and concrete creep, and consequently, the stress on the anchor head that secures the PT tendon also diminishes. This study proposes an automatic detection system to identify tension reduction in a PT tendon using pulsed-eddy-current (PEC) measurement. An eddy-current sensor is installed on the surface of the steel anchor head. The sensor creates a pulsed excitation to the driving coil and measures the resulting PEC response using the pick-up coil. The basic premise is that the tension reduction of a PT tendon results in stress reduction on the anchor head surface and a change in the PEC intensity measured by the pick-up coil. Thus, PEC measurement is used to detect the reduction of the anchor head stress and consequently the reduction of the PT tendon force below a certain threshold value. The advantages of the proposed PEC-based tension-reduction-detection (PTRD) system are (1) a low-cost (< \$ 30), low-power (< 2 Watts) sensor, (2) a short inspection time (< 10 seconds), (3) high reliability and (4) the potential for embedded sensing. A 3.3 m long full-scale monostrand PT tendon was used to evaluate the performance of the proposed PTRD system. The PT tendon was tensioned to 180 kN using a custom universal tensile machine, and the tension was decreased to 0 kN at 20 kN intervals. At each tension, the PEC responses were measured, and tension reduction was successfully detected.

Keywords: post-tensioning tendon; tension reduction detection; pulsed-eddy-current measurement; post-tensioned concrete; nondestructive testing and evaluation

1. Introduction

During the past few decades, precast concrete girders have become popular due to their advantages in rapid construction and enhanced quality control (Sofia *et al.* 1994, Hieber *et al.* 2005, Hanna *et al.* 2009). Surveys indicate that approximately 50 percent of bridges constructed in the United States are precast/pre-stressed concrete bridges (Ma *et al.* 2004).
Post-tensioning (PT) is the most common approach to threading multiple segments of precast concrete girders at a construction site. During PT, a bundle of high-strength prestressing strands (also known as a tendon) is inserted into a duct previously placed in a precast concrete girder. As shown in Fig. 1, one end of the inserted tendon is fixed using anchoring instruments, and the other end is pulled using a hydraulic jack. As a result of the tension applied to the tendon, the precast girder segments are subjected to compression, which enables them to behave as a single integrated unit. In recent, various researches to investigate the behavior of unbonded PT tendon have been progressed which is advantageous comparing to the conventional

bonded PT tendon (Lee *et al.* 2011, Mohammed *et al.* 2017) at the aspects of construction and maintenance of a pre-stressed concrete.

The tension applied to PT tendons diminishes mainly for two groups of reasons: (1) immediate loss and (2) time-dependent loss (Tadros *et al.* 2003). Elastic shortening, concrete shrinkage, duct friction and wedge set comprise the first group, whereas concrete creep, steel relaxation and corrosion comprise the second group. Excessive tension reduction compromises bridge integrity and may result in the catastrophic collapse of the entire bridge system. In fact, a number of bridges have collapsed due to a reduction of the PT tendon force: Ynys-y-Gwas Bridge, UK (1985), Melle Bridge, Belgium (1992), Koror-Babelthuap Bridge, Palau (1996), Saint Stefano Bridge, Italy (1999) and Lowe's Motor Speedway Footbridge, USA (2000) (Woodward and Williams 1988, Goins 2000, Proverbioi and Ricciardi 2000).

Several techniques have been proposed to evaluate the tension of a steel cable. Wang *et al.* (2005) estimated the tension force of a cable by measured the electromagnetic response of the cable. Because the electromagnetic testing device is bulky and consumes a substantial amount of power, this technique is unsuitable for PT tendons embedded inside concrete. Kim *et al.* (2012) developed a smart tendon by inserting Fiber Bragg Grating (FBG) optical fibers into a tendon's central wire. The tendon force is evaluated by measuring the FBG strain. The fabrication

---

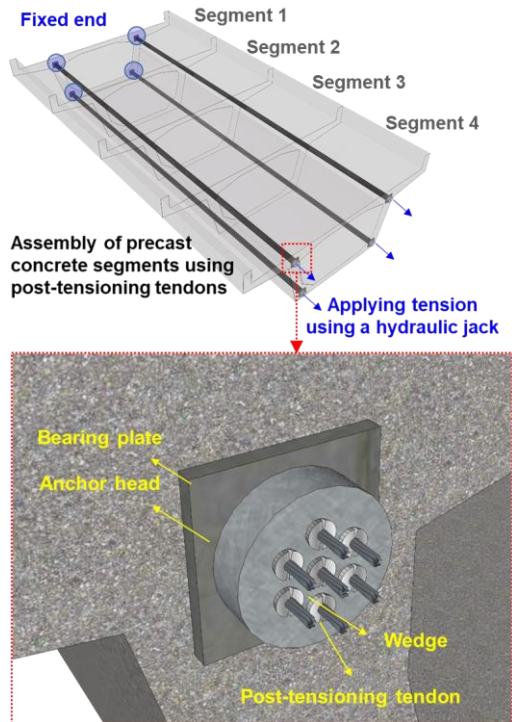*Corresponding author, Professor
 E-mail: hoonsohn@kaist.ac.kr
[a]Ph.D. Student

Fig. 1 Assembly of precast concrete girders using PT tendons (Kim *et al.* 2017)

Fig. 2 Configuration of the ESCs used in the proposed PTRD system: Three ECSs are installed on the surface of an anchor head to measure the alteration of PEC response due to tension change in a PT tendon

of the smart tendon (i.e., drilling a hole into a wire and inserting optical fibers in the hole) is challenging, and the cost associated with optical-fiber sensing is relatively high. Abdullah *et al.* (2015) attached strain gauges to the anchor head of a PT tendon and investigated the relationship between the strain and the number of disconnected wires. However, the sensitivity of the strain reading was only validated to identify fully disconnected wires. A piezoelectric transducer was used to generate ultrasonic waves along a tendon, and the amount of wave energy that leaked from a central wire to peripheral wires was used to assess tension alteration (Bartoli *et al.* 2011). Because ultrasonic waves must propagate from one end of a tendon to the other and attenuate significantly along the tendon, this technique cannot be applied to a long tendon, particularly one embedded in concrete. In addition, attaching piezoelectric transducers to a tendon is difficult. Kim *et al.* (2017) installed an eddy-current sensor (ECS) on the outer surface of a wedge holding a PT tendon and demonstrated that the intensity of the induced eddy current is closely related to the tension of the PT tendon. By employing the frequency-swept sinusoidal input to the ECS, alterations of the frequency responses of the eddy-current at various tensions were investigated. This approach only provided a qualitative warning of excessive tendon force reduction, without a quantitative estimation of the tension force.

Recently, a pulsed eddy current (PEC) measurement has been used for stress evaluation. Morozov *et al.* (2010) successfully evaluated the tensile stress in aluminum alloys by measuring PEC response alterations. Habibalahi and Safizadeh (2014) attempted to use PEC responses to estimate the subsurface residual stress of the annealed
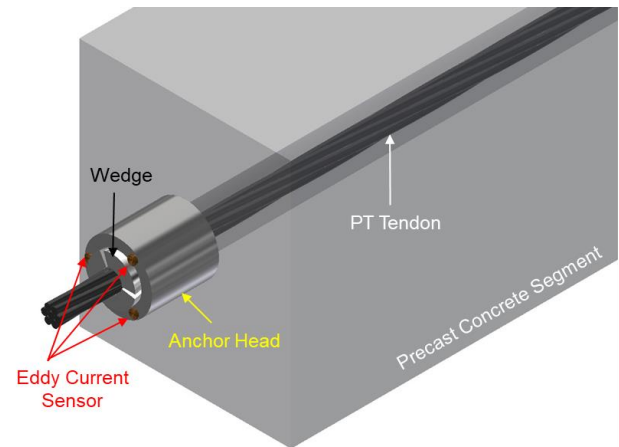
aluminum alloy. Zhou *et al.* (2017) measured PEC responses using a specially-designed U-shaped sensor, and detected the tensile stress variations in a ferromagnetic material. Further, the reliability of PEC based nondestructive testing has been improved by alleviating the effect of a lift-off distance on PEC measurements (Tian *et al.* 2005, Yang *et al.* 2010, He *et al.* 2013) and by applying various signal processing techniques (Yang *et al.* 2009, Qiu *et al.* 2013, Chen *et al.* 2014,).

In this study, an automatic detection system is developed based on PEC measurement to reliably signal the tension reduction of in-service PT tendons. A compact ECS is designed and attached to the anchor head surface of the PT tendon, which is embedded inside precast concrete girders. Power consumption is minimized by optimizing the design of the ECS and employing PEC measurement. An automated warning algorithm is developed to signal tension reduction below a certain threshold value. To the best knowledge of the authors, the developed pulsed-eddy-current-based tension-reduction-detection (PTRD) system is the first system that can detect the tension reduction of PT tendons embedded in precast concrete girders. Additionally, the developed PTRD system is low cost and consumes little power, making it attractive for embedded sensing and integration with power-harvesting techniques.

Section 2 introduces the hardware used in the proposed PTRD system and describes its working principle. A numerical stress analysis of the PT anchorage is performed, and the fundamentals of PEC measurement are explained. Section 3 describes an automatic PTRD algorithm. The performance of the developed PTRD system is experimentally tested using a full-scale monostrand PT tendon in Section 4. Section 5 concludes with a summary and discussion.

2. Development of a PEC-based tension-reduction-detection (PTRD) system

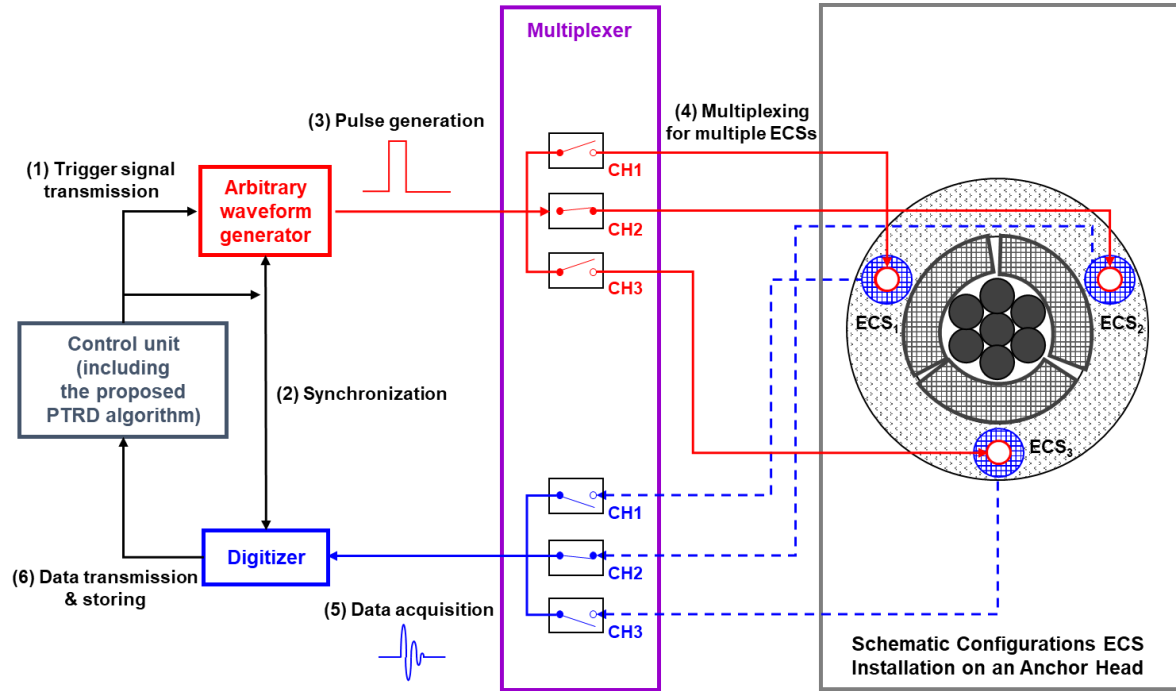### 2.1 Overview of the PTRD system

Fig. 3 Developed PTRD hardware consisting of an AWG, a digitizer, a multiplexer, a control unit, and ECSs

The proposed PTRD system evaluates the tension reduction in a PT tendon by measuring the PEC response on a PT anchorage. In Fig. 2, a PT tendon is fixed at one end of a precast concrete segment using a wedge and an anchor head. The basic assumption of the PTRD system is that tension reduction in a PT tendon results in stress reduction on the anchor head and consequently the alteration of the PEC response. As shown in Fig. 2, the PTRD system employs three ECSs attached on the PT anchorage and measures the PEC response to detect stress variation on the anchor head and tension reduction. Once the tendon force decreases below a threshold value, the PTRD system sends out a warning signal. The detailed working principle of the PTRD system is described in Section 2.3, with the numerical stress analysis on the PT anchorage, an introduction to the Villari effect, and an explanation of PEC measurement.

2.2 Configuration of the PTRD hardware

The developed PTRD hardware in Fig. 3 consists of an arbitrary waveform generator (AWG), a multiplexer, a digitizer and a control unit. The AWG conducts digital-to-analog conversion with 16-bit resolution, 100 MHz sampling frequency, and ± 6 V output range. The digitizer is responsible for converting the input analogue signal to a digital signal with 14-bit resolution, 1.22 mV sensitivity and ± 10 V input range, and 100 MHz maximum sampling frequency. The multiplexer contains 16 channels with a frequency bandwidth of 500 MHz and selectively connects the AWG and the digitizer to multiple ECSs. The control unit has a 2.3 GHz processor and 4 GB RAM, and the hardware controls are manipulated using the LabVIEW program in the control unit.

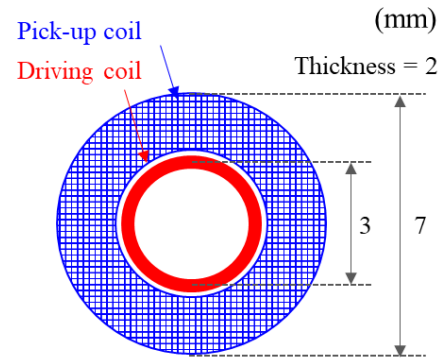The working principle of the hardware shown in Fig. 3

Fig. 4 Proposed ECS design with dimensions

Table 1 Material properties of a PT tendon, a wedge and an anchor head used for FE simulation. (Lee *et al.* 2017)

	PT Tendon	Wedge (SCM 415)	Anchor Head (SM 45C)
Young's Modulus [GPa]	195	200	210
Poisson Ratio	0.30	0.29	0.27
Density [kg/m^3]	7850	7850	7850
Ultimate Strength [MPa]	392	418	476
Yield Strength [MPa]	628	616	657

is as follows. First, the control unit sends a trigger signal to the AWG and the digitizer for time synchronization. A driving pulse generated by the AWG is transferred to the driving coil of the first ECS, and the induced voltage in the pick-up coil of the ECS is transmitted to the digitizer. The digitizer converts the transmitted analog signal to a digital format with a pre-determined sampling frequency, and it is stored in the control unit. This procedure is repeated for the second and third ECSs using the multiplexer. The PTRD
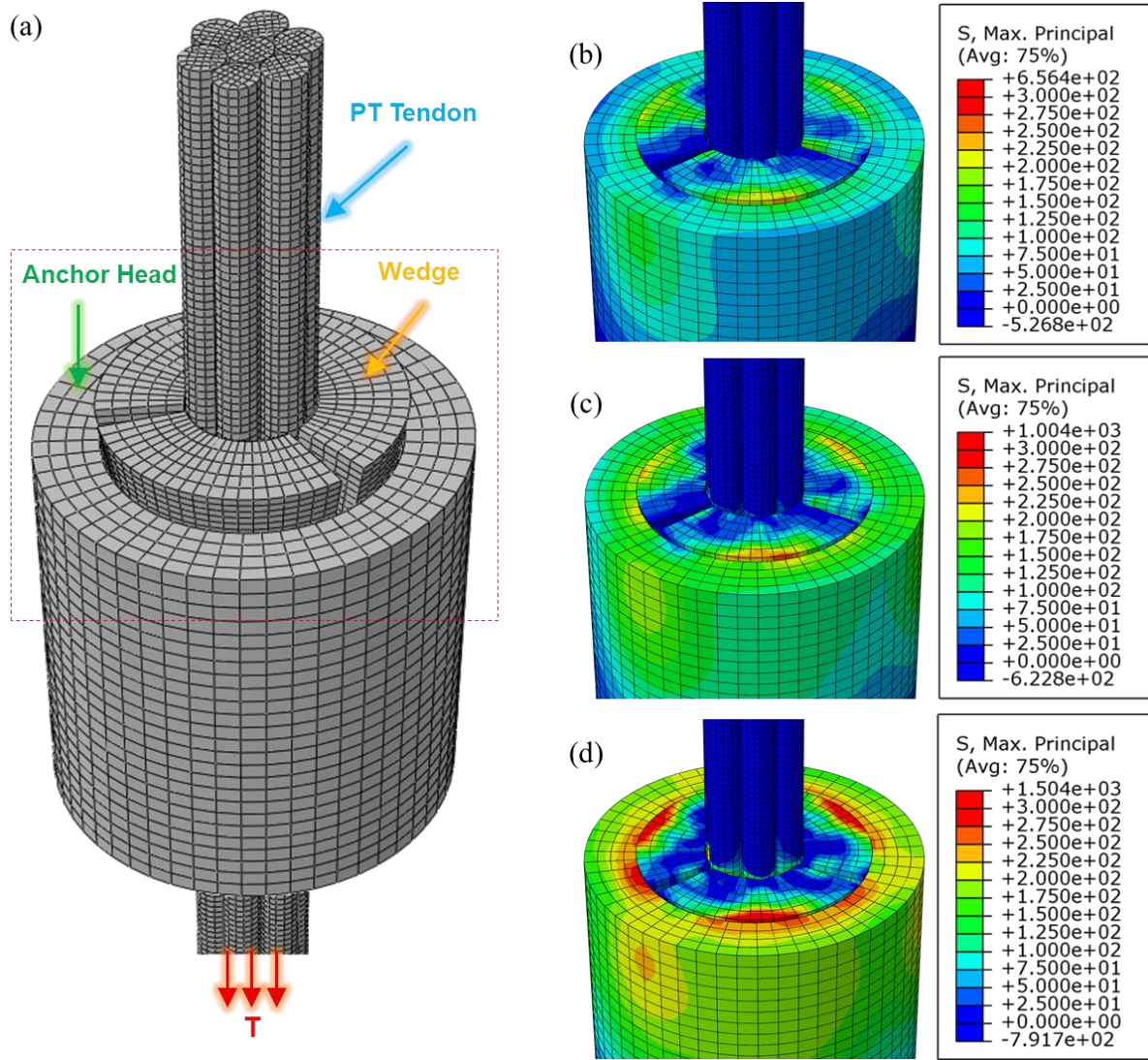
Fig. 5 FE analysis of stress distribution on PT anchorage holding a PT tendon: (a) three-dimensional FE model; (b) stress distribution at T = 60 kN, (c) T = 120 kN, and (d) T = 180 kN

algorithm in the control unit is applied to the measured PEC responses from the ECSs and signals excessive tension reduction.

A compact ECS with a driving coil located inside a pick-up coil is designed (Fig. 4). The inner driving coil has a diameter of 3 mm, and this 60-turn driving coil is fabricated by stacking a 0.1-mm diameter copper wire up to 2 mm. The outer pick-up coil has a diameter of 7 mm and 300 turns made by stacking a 0.1-mm diameter copper wire up to 2 mm. Because of the limited size of the anchor head used in this study, the diameter of the propsoed ECS was restricted to 7 mm. To increase the sensing area for the secondary magnetic field and improve the sensitivity to tension variation, the pick-up coil was placed outside of the driving coil (Xu *et al.* 2011). The electrical resistance, inductance and impedance (at 10 kHz) of the driving and pick-up coils were ascertained to be 1.49 / 11.2 Ω, 11.52 / 400.8 μH and 1.87 / 27.6 Ω, respectively.

2.3 Working principle of the PTRD system

2.3.1 Relationship between stress on the PT anchorage and tension in a PT tendon

The relationship between stress reduction at a PT anchorage and tension reduction in a PT tendon is numerically investigated using the commercial finite element (FE) analysis program ABAQUS Standard 6.13. Full-scale three-dimensional FE models of a wedge, an anchor head and a monostrand PT tendon are shown in Fig. 5 (a). Their material properties, such as Young's modulus, Poisson's ratio and density, are listed in Table 1 (Lee *et al.* 2017). Note that the helical steel wires in an actual PT tendon are replaced with straight wires for computational simplicity. The produced FE models are meshed using a hexahedral element, and the mesh sizes of the wedge, the PT tendon and the anchor head are set to 0.25, 0.25 and 0.5 mm, respectively. A rough contact is assigned to the PT tendon and wedge interface and a frictional coefficient of 0.1 to the wedge and anchor head interface (Lee *et al.* 2017). Here, a rough contact between the PT tendon and the wedge prevents relative slipping by specifying an infinite frictional coefficient. Regarding boundary conditions, the

displacements at the bottom surface of the anchor head are fixed in all directions.

As shown in Fig. 5(a), a tension force T is applied to the free end of the PT tendon up to 180 kN. Figs. 5(b), (c) and (d) show the distribution of stress on the PT anchorage when T equals 60, 120 and 180 kN, respectively. Note that S. Max. Principal in the color bar displays the maximum value of an element among its three principal stresses (σ_1, σ_2 and σ_3). Fig. 5 shows that the alteration of the PT tendon force induces the stress variation on the PT anchorage, and tensile stress is observed on the surface of the anchor head. In particular, the largest stress variation occurs near the contact regions between the anchor head and the wedge pieces. Therefore, the ECSs are placed near these contact regions (Fig. 2).

2.3.2 Villari effect

The Villari effect (also known as the inverse magnetoelastic effect) describes how stress variation in ferromagnetic materials alters the magnetic permeability of such materials (Brown 1965). The effect originates in a magnetic domain that is a basic unit consisting of the ferromagnetic material. The magnetic domain contains its own magnetic moment, and it is randomly aligned in the unstressed state ($\sigma = 0$). However, when a certain level of stress ($\sigma \neq 0$) is introduced, the magnetic domain and its magnetic moment are rearranged, affecting the magnitude of the magnetic permeability (Jiles and Atherton 1986). The following linear Villari effect can be assumed under a low-intensity magnetic field.

$$B = \mathrm{d}\sigma + \mu^\sigma H \qquad (1)$$

where B and H are the magnetic induction and the applied magnetic field strength, respectively. The magnetoelastic coupling is defined through the piezo-magnetic cross-coupling coefficient d. Here, μ^σ is magnetic permeability at a constant stress. According to Eq. (1), change in stress σ results in alternations of the magnetic permeability μ^σ and subsequently the magnetic induction B even under the constant magnetic field strength H.

2.3.3 Fundamentals of pulsed-eddy-current (PEC) measurement

In Fig. 6 (a), an ECS is placed on the surface of the anchor head, and a square driving pulse is applied to the driving coil to generate magnetic field H_1 around the driving coil. Then, magnetic induction B_s ($= \mu_s H_1$) and a PEC are induced on the anchor head surface. Here, μ_s is the magnetic permeability of the anchor head. Sequentially, the produced PEC on the anchor head generates H_2 near the surface, and the voltage V is induced in the pick-up coil following Faraday's induction law.

$$V = -\frac{d\left(\mu_0 H_1 + \mu_0 H_2\right)A}{dt} \qquad (2)$$

where A is the cross-sectional area of the ECS and μ_0 is the magnetic permeability in vacuum ($4\pi \times 10^{-7}$ H/m). Note that H_2 is the function of PT tendon force T and magnetic permeability μ_s of the anchor head (i.e., $H_2 = f(\mu_s, \text{T})$). The voltage V in the pick-up coil is generated only at the rising
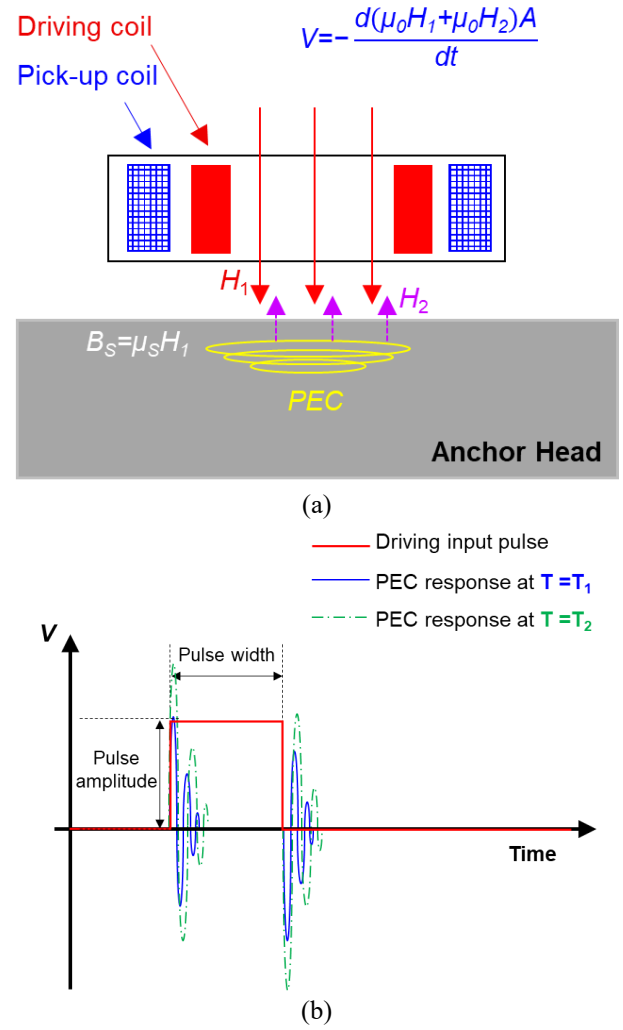

(a)

(b)

Fig. 6(a) PEC measurement using an ECS installed on the surface of the anchor head; (b) alteration of the PEC response and the corresponding induced voltage V in the pick-up coil due to tension change in a PT tendon

and falling edges of the input pulse because rapid change of H_1 only occurs at these edges.

In Fig. 6(b), when the tension in a PT tendon changes from T_1 to T_2, the relative magnetic permeability μ_s of the anchor head alters due to the Villari effect. This alteration of μ_s subsequently changes the magnitude of B_s and the PEC response on the anchor head, affecting the generation of H_2. Through Eq. (2), by acquiring the voltage V in the pick-up coil, the PEC response on the anchor head can be measured to evaluate the tension reduction in the PT tendon.

3. Development of an Automated Tension Reduction Detection Algorithm

Fig. 7 provides an overview of the developed PTRD algorithm, which consists of four steps: (1) initial PEC measurement before applying tension to a PT tendon once the PT tendon is installed on a precast concrete girder, (2) PEC measurement after applying the initial maximum tension to the PT tendon via hydraulic jacking, (3)
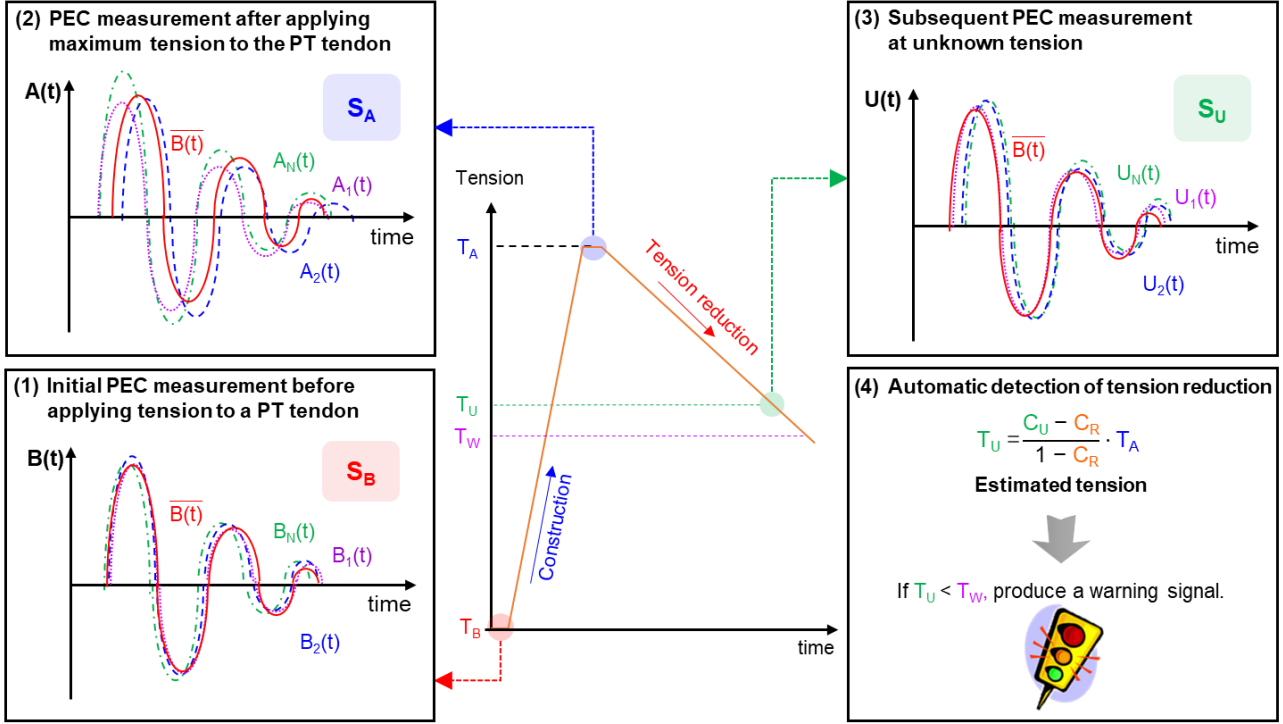
Fig. 7 Overview of the developed PTRD algorithm: (1) initial PEC measurement before applying tension to a PT tendon; (2) PEC measurement after applying the maximum tension to the PT tendon; (3) subsequent PEC measurement at unknown tension; (4) automatic detection of tension reduction
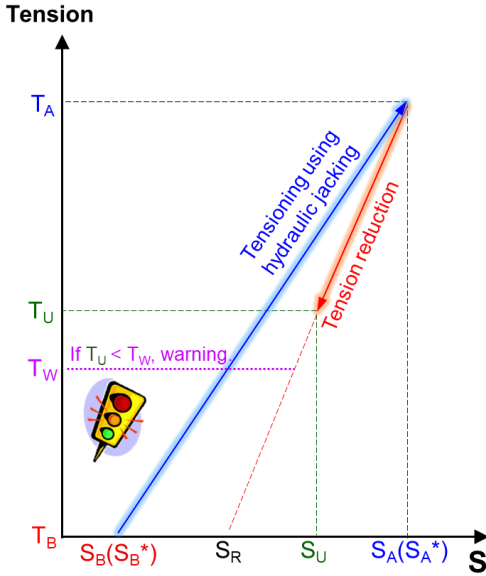

Fig. 8 Relationships between the tension force and the standard deviation at different tension levels

subsequent PEC measurement at unknown tension during periodic inspection, and (4) automatic detection of tension reduction.

(1) Initial PEC measurement before applying tension to a PT tendon

Once precast concrete girders are assembled, the proposed ECSs are installed at one end of the PT tendon. Then, the PEC responses are measured N times before tension is applied to the tendon ($T=T_B=0kN$), and the

standard deviation S_B is computed using the following Eq. (3).

$$S_B = \left(\sum_{i=1}^{N} \sum_{j=1}^{M} \left(B_i \left(j \cdot \Delta t \right) - \overline{B} \left(j \cdot \Delta t \right) \right)^2 / M \cdot N \right)^{1/2} \qquad (3)$$

where $B_i(t)$ (i = 1, 2, ..., N) are the PEC responses measured before applying tension. $\overline{B(t)}$ ($= \sum_{i=1}^{N} B_i(t) / N$) the averaged response, Δt denotes the sampling interval of each PEC response, and M denotes the number of sample points in each PEC response.

(2) PEC measurement after applying the maximum tension to the PT tendon

Once the initial PEC measurement is complete, the maximum tension is applied to the opposite end of the PT tendon ($T=T_A=T_{max}$), where no ECS is installed, using a hydraulic actuator. Then, PEC measurements and the calculation of the standard deviation are repeated as before.

$$S_A = \left(\sum_{i=1}^{N} \sum_{j=1}^{M} \left(A_i \left(j \cdot \Delta t \right) - \overline{B} \left(j \cdot \Delta t \right) \right)^2 / M \cdot N \right)^{1/2} \qquad (4)$$

where $A_i(t)$ (i = 1, 2, ..., N) are the PEC responses measured at the maximum tension. Note that S_A was computed with respect to $\overline{B(t)}$ rather than $\overline{A(t)}$. Thus, S_A is always larger than S_B.

(3) Subsequent PEC measurement at unknown tension

After the completion of construction, the tension applied to the tendon diminishes over time due to, e.g., steel corrosion, concrete shrinkage and creep. As shown in step

(3) of Fig. 7, PEC measurements, $U_i(t)$ ($i = 1, 2, \ldots, N$), are again repeated N times during periodic inspection, and S_U is computed as follows.

$$S_U = \left(\sum_{i=1}^{N} \sum_{j=1}^{M} \left(U_i \left(j \cdot \Delta t \right) - \overline{B} \left(j \cdot \Delta t \right) \right)^2 / M \cdot N \right)^{1/2} \qquad (5)$$

In theory, S_U will always range between S_B and S_A. A smaller S_U value indicates that the tension of the PT tendon has significantly decreased from the initial maximum tension.

(4) Automatic detection of tension reduction

In this final step, the tension at the periodic inspection is estimated, and a warning signal is emitted if the estimated tension falls below a prescribed threshold value.

First, the residual stress coefficient, C_R, is defined in Eq. (6), which was obtained from separate specimen tests using PT tendons identical to those used in the field. An asterisk (*) denotes that the value was acquired in the specimen tests only to investigate the C_R value.

$$C_R = \frac{S_R^* - S_B^*}{S_A^* - S_B^*} \qquad (6)$$

where C_R indicates the level of the residual stress on the anchor head surface once the applied tension is completely removed, and S_R denotes the corresponding standard deviation with respect to $\overline{B(t)}$. It should be noted that, even when the applied tension is completely removed from the PT tendon, a certain level of residual stress remains on the anchor head. Then, the corresponding standard deviation, S_R^*, obtained after tension removal is always larger than S_B^* (Fig. 8). $C_R = 0$ means that the removal of the tension does not reduce the surface stress of the anchor head.

Second, the estimation coefficient, C_U, is computed at a specific inspection interval of the target PT tendon using the S_U obtained from Eq. (5).

$$C_U = \frac{S_U - S_B}{S_A - S_B} \qquad (7)$$

S_U in Eq. (5) was defined as the difference between the PEC response obtained without any loading and the PEC response at the current tension level. Therefore, the standard deviation S_U in Fig. 8 is expected to monotonically increase as the tension increases. The linearity between the tension and the S_U value was experimentally validated through tension testing of a steel plate, and a similar linear trend was reported by Xiu *et al.* (2017). However, the test result is not provided here due to the page limit. Assuming a linear relation between the tension and S_U in Fig. 8, the unknown tension T_U can be estimated as follows.

$$T_U = \frac{C_U - C_R}{1 - C_R} \cdot T_A \qquad (8)$$

Once the estimated T_U value becomes smaller than a user-specified threshold value of T_W, the PTRD system emits a warning signal.

4. Experimental validation

4.1 Experimental setup

The performance of the developed PTRD system was tested with the experimental setup described in Fig. 9. A 3.3 m long monostrand PT tendon with 15.2 mm diameter was inserted into a custom universal tensile machine (UTM). The UTM consists of a $2400 \times 220 \times 220$ mm^3 steel frame, a hydraulic actuator with a load capacity of 250 kN, and a load cell. A through-hole type load cell was used, and its sensing range was from 0 to 300 kN with 0.1 kN accuracy. The readings of the load cell were considered a ground truth-value. A PT anchorage consisting of a wedge and an anchor head (KTA-MA-Type; Korea Total Anchorage, Inc.) was installed at both ends of the tendon. When the wedge and the anchor head were fully assembled, the overall size of the assembly was Φ 45 mm $\times$ 60 mm. The allowable strength of the tendon was 1860 MPa.

An ECS module is installed on the surface of the PT anchorage. Fig. 10 shows front and back views of the proposed ECS module with its size matched with the size of the PT anchorage. The three identical ECSs in Fig. 10 are equally spaced along the circumference with 120 degrees separation between two adjacent ECSs. To facilitate attachment to the PT anchorage, three permanent magnets are installed on the ECS module. The magnets are also used to maintain the distance between an ECS and the surface of an anchor head constant. Each driving and pick-up coil is linked to the AWG and digitizer of the developed PTRD system using SMA (SubMiniature, version A) connectors. The driving coil of the ECS was excited by a 1.6 V pulsed signal with 100 μs duration. The data acquisition time from the falling edge of the driving pulse was 12 μs, and the sampling frequency was 30 MHz. The power consumption of the ECS was estimated to be 1.37 W ($= V^2 / |Z| = (1.6 \text{ V})^2 / 1.87 \, \Omega$)). The penetration depth of the produced PEC can be computed using the following equation (Mottl 1990).

$$\delta = \sqrt{\frac{\rho}{f \pi \mu_r \mu_0}} \qquad (9)$$

where f denotes the driving frequency applied to the driving coil in Hz, and ρ and μ_r represent the electric resistivity in $\Omega \cdot$m and relative magnetic permeability of a target material, respectively. μ_0 is the magnetic permeability in vacuum ($4\pi \times 10^{-7}$ H/m). In the computation of the penetration depth, δ as the pulse width was 100 μs, its cut-off frequency was 10,000 Hz ($= 1/100$ μs). The ρ and μ_r values of the anchor head steel were $6.9 \ 10^{-7} \, \Omega \cdot$m, and 1000, respectively. Then, the penetration depth was estimated to be around 130 μm. The sensitivity of the ECS was evaluated to be approximately 8.5 mV / 50 MPa ($=$ (voltage variation at the first peak)/(stress variation)) based on tension testing of the aforementioend steel plate.

First, the C_R value was estimated by loading and unloading tests of two identical but independent PT tendons. The PEC responses were repeatedly obtained 10 times (i.e., N = 10) before applying tension ($T = T_B$), after applying the maximum tension of 180 kN ($T = T_A$), and after the complete removal of tension ($T = 0$). Then, the CR value was computed using Eq. (6). Second, two additional PT tendons were prepared to validate the performance of
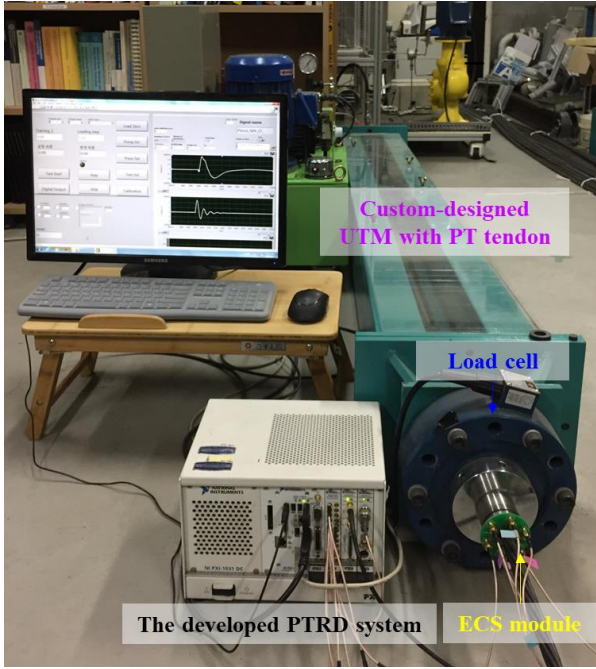
Fig. 9 Experimental setup to validate the performance of the developed PTRD system. A maximum tension of 180 kN is applied to a monostrand PT tendon using a UTM. Then, the tension is gradually reduced to 0 kN with a 20 kN interval

Fig. 10 Front and back views of the ECS module including three identical ECSs with magnets

the PTRD system. In this test, the PEC responses were measured at 9 different tension levels, which ranged from 160 kN to 0 kN at a 20 kN interval. The measured PEC responses were analyzed to estimate the corresponding tension values and detect tension reduction below a threshold value using the PTRD algorithm described in Section 3.

4.2 Experimental results

The installed ECS module generates a pulsed input and measures the corresponding PEC response on the anchor head. The abrupt alteration of the magnetic field H caused by a pulsed input at the driving coil produces a PEC on the surface of the anchor head. Tension reduction in a PT tendon reduces the stress on the anchor head and influences the intensity of the produced PEC response. Fig. 11(a) shows the PEC response measured at the falling edge of the pulsed input, and Fig. 11(b) enlarges the response near the first peak response. Fig. 11(b) shows that the amplitude of the PEC response increases as the applied tensions increases. However, when the applied tension is removed again (T = 0 kN), the amplitude of the PEC response does not shrink back to the original amplitude because of the residual stress on the anchor head. The effect of the residual stress is taken into consideration by the residual stress coefficient C_R defined in Eq. (6). The C_R value was estimated by loading and unloading tests of two identical but independent monostrand PT tendons. S_A*, S_B* and S_R* were computed using Eqs. (3), (4) and (5), respectively. Table 2 summarizes the values obtained from these two tendon experiments. The average C_R value, $\overline{C_R}$, was 0.838, which implies that approximately 83.8% of the tensile
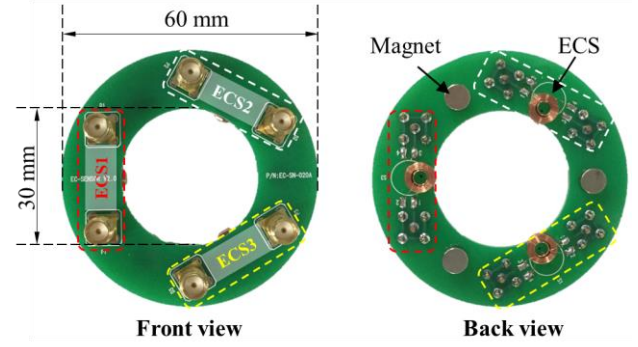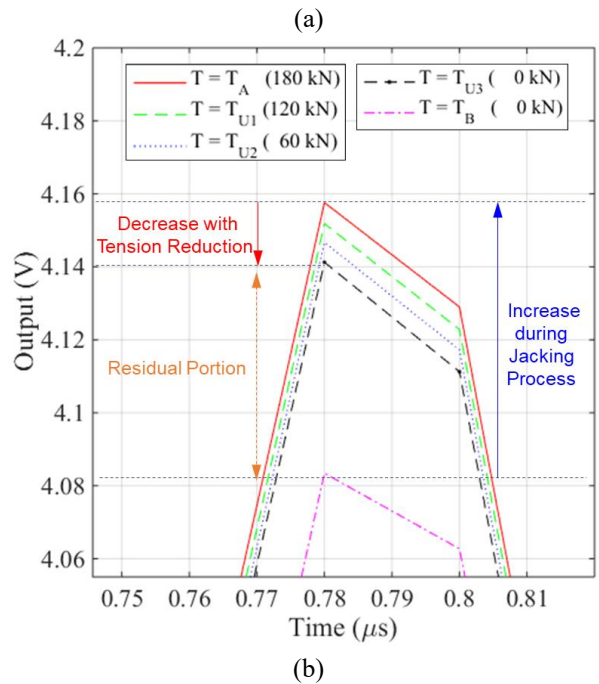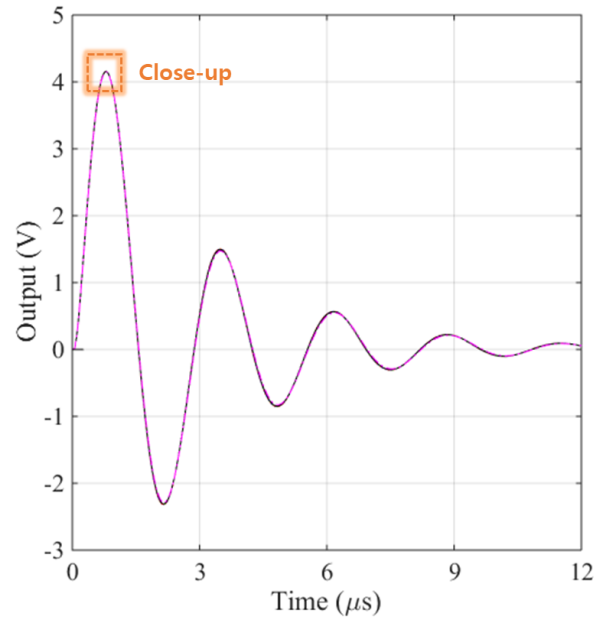

(a)

(b)

Fig. 11 PEC measurements at various tension levels: (a) PEC response at the falling edge of the pulsed input; (b) close-up near the first peak response

Table 2 C_R values estimated from two tendon experiments

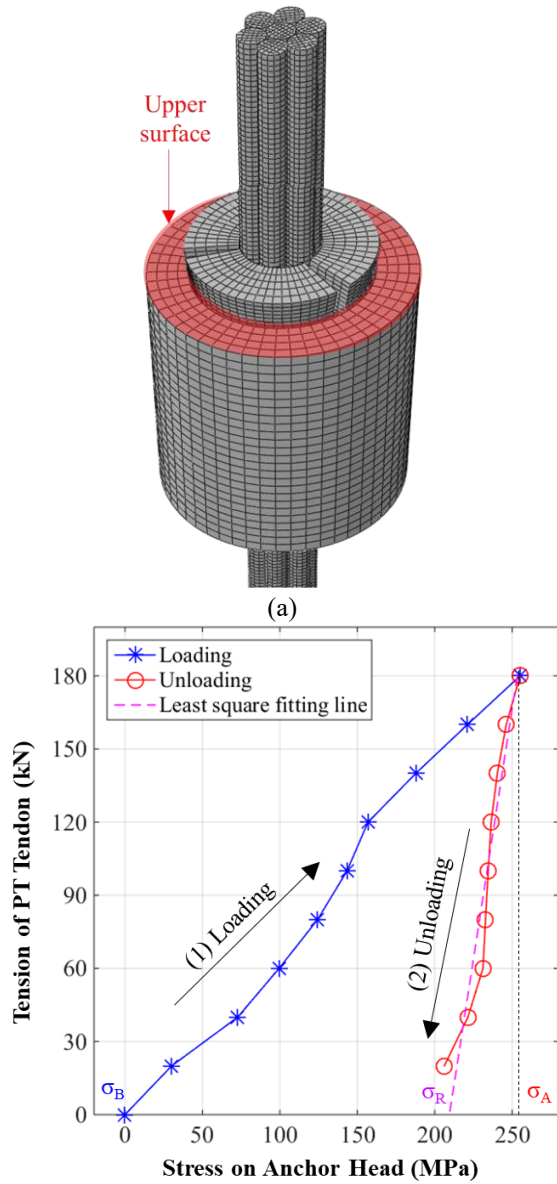|		S_A	S_B	S_R	C_R	$\overline{C_R}$
	ECS#1	0.00371	0.00046	0.00313	0.82134	
1st PT tendon	ECS#2	0.00396	0.00053	0.00338	0.83095	0.844
	ECS#3	0.00410	0.00050	0.00367	0.88072	
	ECS#1	0.00451	0.00051	0.00372	0.80245	
2nd PT tendon	ECS#2	0.00349	0.00048	0.00305	0.85382	0.832
	ECS#3	0.00450	0.00047	0.00386	0.84107	
			$\overline{C_R}$			0.838

(a)

(b)

Fig. 12 Evaluation of C_R value through numerical simulation: (a) 3D FE model of a PT anchorage; (b) the relation between the tension of a PT tendon and the stress on the anchor head during loading and unloading

stress produced by the maximum tension remains even when the tension is removed.
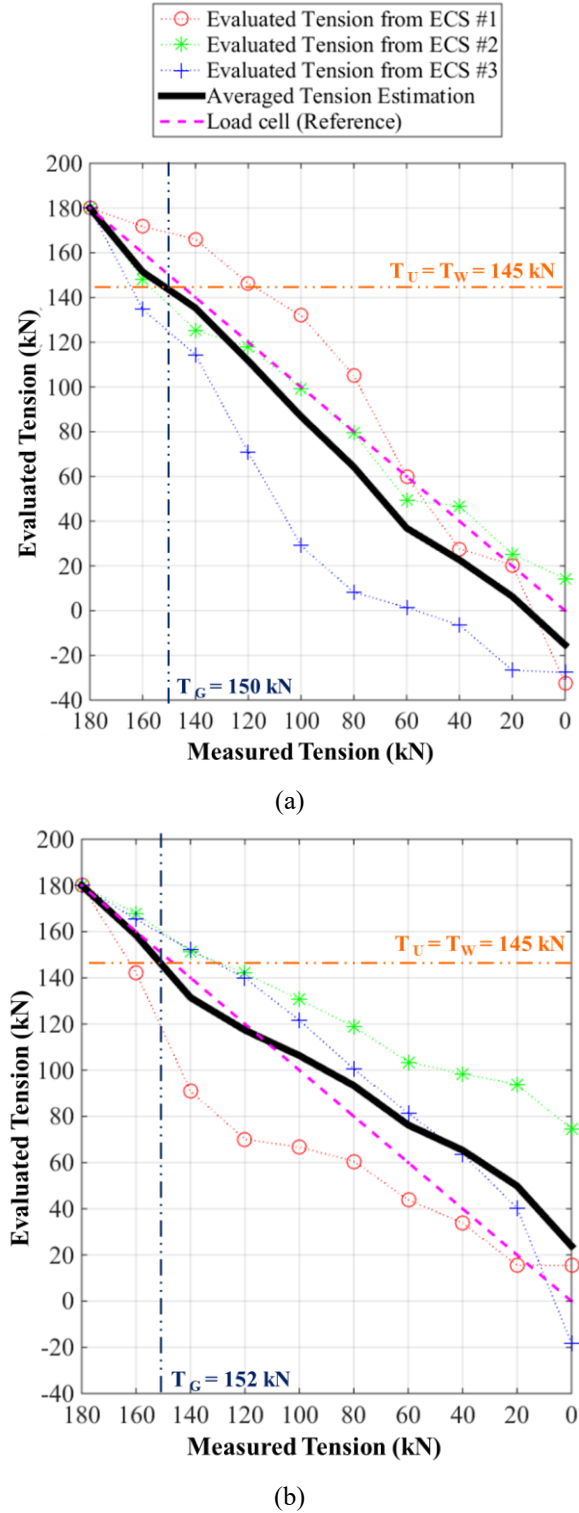

(a)

(b)

Fig. 13 Comparison between the reference tension (magenta dash line) measured by a load cell and the average tension (black solid line) estimated by the proposed PTRD system: (a) first and (b) second tests. ($C_R = 0.838$ from the specimen tests is used.)

The C_R value is also evaluated through the numerical simulation of the 3D FE model developed in Section 2.3.1. The PT tendon force was increased to 180 kN and reduced to 0 kN with a 20 kN increment. The average stress over the

upper surface of the anchor head shown in Fig. 12(a) was calculated. Fig. 12(b) shows the relation between the PT tendon force and the average stress on the anchor head during loading (the blue solid line with asterisks) and unloading (the red solid line with circles). The stress at T = 0 kN during the unloading phase was not computed because of numerical instability caused by insufficient contact between the wedge and the anchor-head model. Instead, the residual stress at T= 0 kN was extrapolated after fitting a straight line to the simulated datapoints at T = 20, 40, …, and 180, as denoted by the magenta dotted line in Fig. 12(b). In Fig. 12(b), σ_B, σ_A and σ_R represent the average stress on the upper surface of the anchor head before loading, at maximum tension and after unloading, respectively. Their values were estimated to be 0, - 255.1 and -209.5 MPa, respectively. The corresponding C_R value of 0.821 is in good agreement with the C_R value of 0.838 obtained from the experiments.

Next, the performance of the developed PTRD system was examined by testing two additional tendons. All the test configuration and procedures were identical to those of the previous tests unless specified. Fig. 13 compares the tension measured by the load cell (the magenta dash line) and the average tension (the black solid line) estimated by the proposed PTRD system. Here, the average tension is calculated by averaging the tensions estimated from three ECSs

$$T_U = (T_{ECS1} + T_{ECS2} + T_{ECS3})/3 \qquad (9)$$

where T_{ECS1}, T_{ECS2} and T_{ECS3} denote the tension evaluated from ECS #1, #2 and #3, respectively. Because stress variation is expected over the anchor head surface as implied by the numerical simulation shown in Fig. 5, the average tension was estimated from the three ECSs. Good agreement between the measured and estimated tensions can be observed in Fig. 13. Because a 20% tension reduction is typical within the allowable range (Aalami 2000, Zia *et al.* 1979), T_W was set at 145 kN ($\approx$ 180 kN × 0.8). Therefore, when T_U reaches 145 kN, the system emits a warning signal. In Fig. 13, the warning signal was produced when the actual tension was 152 kN and 150 kN for first and second tendons, respectively. Although the PTRD system overestimated the tension reduction as much as 4.17% and 2.78% for first and second PT tendons, respectively, it could at least provide an early warning of tension reduction.

5. Conclusions

In this paper, a pulsed-eddy-current-based tension-reduction-detection (PTRD) system is developed for monitoring post-tensioning (PT) tendons, commonly used for precast concrete girders. The PTRD system uses a low-cost, low-power eddy-current sensor (ECS) module installed on the surface of an anchor head and measures a pulsed-eddy-current (PEC) response. Tension reduction in a PT tendon causes stress variation on an anchor head and consequently changes the PEC response due to the Villari effect in ferromagnetic materials. The proposed PTRD

system detects tension reduction by measuring PEC responses.

The performance of the PTRD system was experimentally validated by testing two monostrand PT tendons. A maximum tension of 180 kN was applied to the tendons, and the tension was gradually reduced from 180 kN to 0 kN at 20 kN interval. The threshold value for tension reduction warning was set to 145 kN, which corresponds to approximately 80 % of the maximum tension. In the two tendon tests, the warning was emitted when the actual tension was 152 kN and 150 kN for the first tendon and the second tendon, respectively. Although the PTRD system overestimated tension reduction approximately 5%, the system provided early warning of tension reduction.

The unique contributions of this study are (1) the use of PEC measurement on the anchor head for detecting reduction of a PT tendon force and (2) numerical and experimental validations of the relationship between the PT tendon force and the stress on the PT anchorage. The employment of PEC measurements offers (1) rapid tendon inspection in less than 10 seconds, and (2) a deeper penetration depth (over 130 μm) and an improved sensitivity to tendon force variation than the previous sweeping eddy current technique (Kim *et al.* 2017).

Compared to an electromagnetic (EM) sensor used for cable tension measurement, the PTRD system has the following differences and advantages. First, the main difference is the location where each sensor is installed. The EM sensor encases a steel cable (or tendon in our case), and generates a magnetic field directly on the steel cable and measures the induced electromotive force on the cable. On the other hand, the ECS module of the PTRD system is installed on the anchor head, which is more convenient to access during tendon installation. Second, the proposed PTRD system requires less than 1% of the power required to operate the EM sensor. The EM sensor demands hundreds of Watts to create a high-intensity magnetic field (over 10,000 Oe) so that the target specimen can be magnetically saturated. On the other hand, the proposed PTRD system needs only a few Watts since the cable tension is estimated under a low-intensity magnetic field (less than 1,000 Oe).

Prior to field deployment of the proposed PTRD system, several issues must be addressed. First, for the full embedment of the ECS module and the data-processing unit inside precast concrete girders, the development of a wireless power and data transmission technique through concrete must be completed. Second, the current technique is only applicable to ungrouted PT tendons. Further investigation is warranted for grouted tendons. Third, a more reliable tension estimation technique is required to compensate the variation of the PEC measurements caused by environmental variations (e.g., temperature, humidity and corrosion on the anchor head) in the field.

Acknowledgments

by the Ministry of Land, Infrastructure and Transport (MOLIT) of the South Korean government.

CC

References

Abdullah, A.B.M., Rice, J.A. and Hamilton, H.R. (2015), "Wire breakage detection using relative strain variation in unbonded posttensioning anchors", *J. Bridg. Eng.*, **20**, 04014056.

Bartoli, I., Salamone, S., Phillips, R., Lanza Di Scalea, F. and Sikorsky, C.S. (2011), "Use of interwire ultrasonic leakage to quantify loss of prestress in multiwire tendons", *J. Eng. Mech.*, **137**, 324-333.

Brown Jr, W.F. (1965), "Theory of magnetoelastic effects in ferromagnetism", *J. Appl. Phys.*, **36**(3), 994-1000.

Goins, D. (2000), "Motor speedway bridge collapse caused by corrosion", *Mater. Perform.*, **37**, 18-19.

Hanna, K.E., Morcous, G. and Tadros, M.K. (2009), "Transverse post-tensioning design and detailing of precast, prestressed concrete adjacentbox-girder bridges", *PCI J.*, **54**(4), 160-174.

Hieber, D.G., Wacker, J.M., Eberhard, M.O. and Stanton, J.F. (2005), *State-of-the-Art Report on Precast Concrete Systems for Rapid Construction of Bridges*, Report No. WA-RD 594.1, Washington State Transportation Center (TRAC), University of Washington, U.S.A.

Jiles, D.C. and Atherton, D. L. (1986), "Theory of ferromagnetic hysteresis", *J. Magn. Magn. Mater.*, **61**(1-2), 48-60.

Lee, J., Kim, J.M. and Sohn, H. (2017), "Magnetostriction analysis of a post tensioning tendon system under varying tension forces", *Proceedings of the Advances in Structural Engineering and Mechanics (ASEM17)*, Ilsan, Korea, August.

Lee, D.H. and Kim, K.S. (2011), "Flexural strength of prestressed concrete members with unbonded tendons", *Struct. Eng. Mech.*, **38**(5), 675-696.

Ma, Z., Tadros, M.K. and Sun, C. (2004), "Prestressed concrete box girders made from precast concrete unsymmetrical sections", *PCI J.*, **49**(1), 80-90.

Mohammed, A.H. and Taysi, N. (2017), "Modelling of bonded & unbonded post-tensioned concrete flat slabs under flexural & thermal loading", *Struct. Eng. Mech.*, **62**(5), 595-606.

Kim, J.M., Lee, J. and Sohn, H. (2017), "Automatic measurement and warning of tension force reduction in a PT tendon using eddy current sensing", NDT & E Int., **87**, 93-99.

Kim, J.M., Kim, H.W., Park, Y.H., Yang, I.H. and Kim, Y.S. (2012), "FBG sensors encapsulated into 7-wire steel strand for tension monitoring of a prestressing tendon", *Adv. Struct. Eng.*, **15**, 907-917.

Proverbioi, E., and Ricciardi, G. (2000), "Failure of a 40 years old post tensioned bridge near seaside", *Proceedings of the International Conference of Eurocorr*, London, U.K.

Sofia, M.J. and Homsi, E.H. (1994), "Fabrication and erection of precast concrete segmental boxes for baldwin bridge", *PCI J.*, **39**(6).

Tadros, M.K., Al-Omaishi, N., Seguirant, S.J. and Gallt, J.G. (2003), *Prestress Losses in Pretensioned High-Strength Concrete Bridge Girders*, Report No. HCHRP 496, Transportation Research Board.

Woodward, R. and Willians, F. (1988), "Collapse of Ynys-y-Gwas bridge West Glamorgan", *Proceedings of the Institution of Civil Engineers*, **84**, 635-669.

Wang, G., Wang, M.L., Zhao, Y., Chen, Y. and Sun, B. (2005), "Application of EM stress sensors in large steel cables", *Smart Struct. Mater.*, **5765**, 395-406.

Zhao, X. and Lord, D.G. (2006), "Application of the villari effect to electric power harvesting", *J. Appl. Phys.*, **99**, 2014-2017.